Available online at www.sciencedirect.com
ScienceDirect
Ceramics International 34 (2008) 27–35
CERAMICS INTERNATIONAL
www.elsevier.com/locate/ceramint

Modelling of the grain growth and the densification of SnO_2-based ceramics

A. Maître [a,*], D. Beyssen [b], R. Podor [b]

[a] Laboratoire Science des Procédés Céramiques et Traitements de Surface, UMR CNRS 6638, Université de Limoges, 123, Av. Albert-Thomas, F-87060 Limoges Cedex, France
[b] Laboratoire de Chimie du Solide Minéral, UMR CNRS 7555, Université Henri Poincaré Bd des Aiguillettes, BP 239, F-54506 Vandoeuvre-les-Nancy Cedex, France

Received 24 April 2006; received in revised form 21 June 2006; accepted 16 July 2006
Available online 18 September 2006

Abstract

This work consisted in the kinetic study of grain growth and densification processes for SnO_2 and $Sn_{0.94}Zr_{0.06}O_2$ ceramics between 1100 and 1200 °C.

From dilatometric experiments, it appeared that zirconia additions inhibited the final densification rate. For pure SnO_2, the rate limiting step of the densification mechanism would correspond to the grain boundary or volume diffusion. From normal grain growth kinetics, the corresponding limiting step has been identified, i.e. either the surface diffusion in pores or grain boundary diffusion for ZrO_2 free-SnO_2 and $Sn_{0.94}Zr_{0.06}O_2$, respectively.

All of these results permit establishing the corresponding sintering map. For pure SnO_2 ceramic, the experimental data have been well restored by modelling.

Keywords: Sintering; SnO_2; Zirconia; Kinetic; Modelling

1. Introduction

Tin oxide polycrystalline ceramics are n-type semiconductors that have been widely used in humidity and carbon monoxide sensors [1–4], in thin films, solar cells and protective coatings [5–8], as electrodes for electric glass melting furnaces and for electrochromic windows [9,10]. Unfortunately, pure SnO_2 is known to be difficult to densify by natural sintering because of the predominance of non-densifying mechanisms for mass transport, such as surface diffusion and evaporation–condensation [11] which only promote pure coarsening and grain growth.

Using small amounts of sintering additives favours densification of SnO_2-based ceramics. Since O^{2-} ions are the rate-controlling diffusion species, cobalt monoxide additions enhance the tin dioxide densification by increasing the oxygen vacancy number [12].

Otherwise, in the case of specific applications of SnO_2-based materials such as heating electrodes where these materials can be in direct contact with metallic pieces at temperature higher than 700 °C, the using of additives such as ZrO_2 seems to be necessary in order to reduce the tin activity in SnO_2 by dilution of tin by Zr. Recent works [13,14] demonstrated the negative role played by zirconia on the tin dioxide densification. So, the relative density did not exceed 93% for a zirconium content lower than 6 mol% in the $Sn_{(1-x)}Zr_xO_2$ solid solution. This negative effect can be imputed to the elastic distortions due to the zirconium introduction in the tin dioxide lattice and, consequently, the diffusion rate of point defects such as oxygen or cobalt ions is lowered. Nevertheless, the zirconia addition to SnO_2 reduces significantly the volatilisation rate of tin dioxide according to the following equation:for temperature higher than 1400 °C [13].

So, the present work consists in the kinetic study of grain growth and densification for SnO_2-based materials as a function of the ZrO_2 content and sintering temperature. This study will allow the determination of the rate-controlling steps during the $Sn_{1-x}Zr_xO_2$ ceramic sintering. At last, the sintering mechanism modelling for SnO_2-based materials has been achieved as a

* Corresponding author. Tel.: +33 5 55 45 74 63; fax: +33 5 55 45 75 86.
E-mail address: alexandre.maitre@unilim.fr (A. Maître).

0272-8842/$32.00
doi:10.1016/j.ceramint.2006.07.008

function of the zirconium content in tin dioxide solid solution and the sintering temperature.

2. Experimental procedure

2.1. Starting materials

Zirconium, tin dioxide and cobalt monoxide were supplied by GoodFellow™, Cerac™ and Aldrich™, respectively. Their main physical-chemistry characteristics are reported in Table 1.

2.2. Apparatus and experimental conditions

The three powders (ZrO_2, SnO_2, CoO) were mixed in a first step in an agate mortar, in a second step, dispersed in pure ethanol with a Turbula apparatus. The powders were then dried at 120 °C for 12 h.

Discs of 13 mm diameter were uniaxially pressed under 222 MPa pressure. Densities were obtained by the Archimedes method. Theoretical density of the mixture was calculated using the mixing law, the theoretical density of ZrO_2 (5.82 g/cm^3), SnO_2 (6.99 g/cm^3) and CoO (6.45 g/cm^3). Densities of cold pressed samples were equal to about 60% of the theoretical. In order to determine the open porosity ratio, the geometric densities were also measured.

Dilatometric measurements were performed using a Setaram TMA92 dilatometer. The heating rate was kept at 10 °C/min. To obtain a network of points showing the grain growth as a function of time, the samples was sintered in a Nabertherm furnace (LHT 04/17 model). The furnace is brought to the required temperature 1 h before the sample introduction. Sample introduction and removal from the hot zones takes about one minute.

After sintering, the samples were polished to obtain a mirror like surface (Diamond spray 1 μm). Grain boundaries were revealed by thermal etching at 1300 °C during 3 min. Grain size analyses were done using micrographs from scanning electronic microscopy (Philips XL 30 or Hitachi 2500). Image analysis was performed using Scion Corporation Software (Scion Corporation).

2.3. Grain size measurements

The equivalent disc diameter is chosen as a parameter for size evaluation. Sampling representation is a key parameter, which controls the measurement reproducibility and conditions its precision. The minimum number of measurements required for an acceptable precision has been looked for.

Table 2
Mean grain size for different sampling

Number of particles	100	200	300	400	600
Average particle diameter ϕ_m (μm)	1.29	1.40	1.37	1.37	1.34
Relative discrepancy (%)	3.7	4.5	2.2	2.2	Reference

Results in Table 2 shows that for more than 300 grains, the average grain size measurement is good. In a general way, measurement done over 300 grains gives an error of 2%. Each value is taken from at less 10 SEM micrographics for a same sample.

3. Results and discussions

The sintering parameters of $Sn_{1-x}Zr_xO_2$ ceramics were determined from previous works [13]: so, the volatility rate of tin dioxide is negligible under air below 1400 °C. Moreover, the addition of 0.5 mol% of CoO to the initial SnO_2–ZrO_2 mixtures has been systematically performed in order to keep the geometric shape of specimens after thermal treatment and so, to determine the densification ratio. Indeed, the densification rate for SnO_2 with an addition of 0.5 mol% CoO can reach 99% [15–17]. From the SnO_2–ZrO_2 phase diagram [15], it appeared that the $Sn_{1-x}Zr_xO_2$solid solution domain is obtained for zirconia content lower than 10 mol% regardless temperature.

3.1. Grain growth

3.1.1. Grain growth kinetics

In the case of normal growth, the kinetic law governing the grain growth obeys to the following equation:

$$G^m - G_0^m = kt \quad (2)$$

where G is the average grain size at time t, G_0 the initial grain size, k a kinetic constant and m a whole number whose value depends upon the diffusion mechanism which is responsible for sintering.

Eq. (2) was established considering the granulometric distribution similar whatever the period of time. In this hypothesis, the normalized distribution should be invariant as a function of time [18]. Several authors [19,20] were able to show experimentally for ceramic systems the self-similarity of grain size distribution as a function of time. This self-similarity is a result of invariance as a function of time, of each grain class (with a ratio $x = D/D_m$ as constant).

Table 1
Main characteristics of the starting powders

Powder (supplier)	Density (g/cm^3)	Specific area[a] (m^2/g)	Granulometry (μm)	
			From Eq. (2)	By image analysis
SnO_2 (Cerac™)	6.95	16.8	0.5	0.2
ZrO_2 (GoodFellow™)	5.89	6.1	0.2	0.2
CoO (Aldrich™)	6.45	4.4	0.2	1.1

[a] The average grain size of ceramic powders were calculated from the specific surface area determined by BET method with a Sorptomatic 1990 Thermoquest apparatus: $\phi_m = 6/\rho S_{BET}$ where ρ is the powder density (g/cm^3), S_{BET} the specific area (m^2/g).

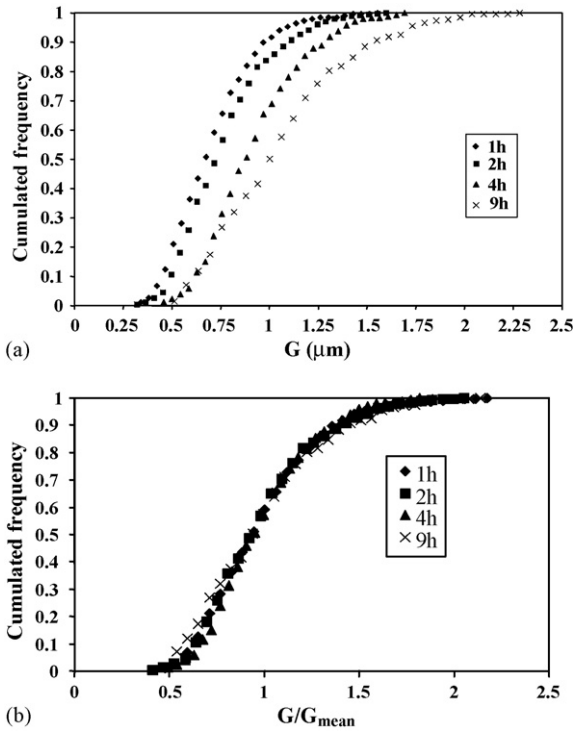

Fig. 1. Conservation of grain size distribution at 1100 °C for $Sn_{0.94}Zr_{0.06}O_2$–0.5 mol% CoO.

A systematic study of the grain growth of $Sn_{0.94}Zr_{0.06}O_2$–0.5 mol% CoO and SnO_2–0.5 mol% CoO ceramics was made while varying the temperature and zirconia content. For $Sn_{0.94}Zr_{0.06}O_2$–0.5 mol% CoO ceramic at 1100 °C, Fig. 1 shows the conservation of grain size distribution as self-similarity. This result clearly demonstrates that the grain growth for $Sn_{0.94}Zr_{0.06}O_2$–0.5 mol% CoO ceramic remains normal under the present experimental conditions. All of the grain distributions follow the same curve, independently of time (0.5–24 h) and temperature (1100, 1150 and 1200 °C), considering both SnO_2–0.5 mol% CoO or $Sn_{0.94}Zr_{0.06}O_2$–0.5 mol% CoO ceramics.

The distribution law can be studied using the estimation of centred moments of the order from 1 to 4. To demonstrate that the distribution obeyed to a log-normal law, the variable change $Z = \ln(G)$ (and also $Z_m = \ln(\bar{G})$) was introduced. For a grain size distribution the calculation of centred moment (μ_p) is often given by

$$\mu_p = \frac{\sum_{i=1}^{q} n_i (\ln(G_i/\bar{G}))^p}{n} \quad (3)$$

where n_i is the number of grains having size G_i, n the total number of grains, q the number of granulometric classes (here $q = 30$).

The four moments are identical for all of the distributions and the corresponding average values have been reported in Table 3. These data enabled to determine the distribution law using Pearson's coefficients. The (β_1 and β_2) coefficients characterise the form of the size distribution: the skewness

Table 3
Values of the centred moments of granulometric distributions

	Centred moments			
	μ_1	μ_2	μ_3	μ_4
Average	−0.09	0.17	−0.02	0.08
S.D.	0.01	0.01	0.01	0.01

($\beta_1 = (\mu_3^2/\mu_2^3)$) measures the asymmetry of the distribution relative to its mean and the degree of peakedness is given by the kurtosis ($\beta_1 = (\mu_4/\mu_2^2)$). The results so-obtained (see Table 3) were approached from the theoretical values $\beta_1 = 0$, $\beta_2 = 3$ confirming the existence of a normal distribution with the following log-normal law:

$$g(x) = \frac{1}{\sqrt{2\mu_2\pi}} \exp\left[-\frac{1}{2}\left(\frac{\ln(x) - \mu_1}{\sqrt{\mu_2}}\right)\right] \quad (4)$$

This model of grain size distribution was often applied to sintered materials [21,22].

The invariance of grain size distribution function versus time allows the separation of the grain size and time variables. The grain distribution function $f(G, t)$ can therefore be represented as the product of two functions

$$f(G, t) = g\left(\frac{G}{\bar{G}}\right) \times h(t) \quad (5)$$

where g function represents the initial distribution of grains and h function gives the evolution of grain growth independently of the grain size. Knowing the grain growth kinetics from the mean grain size ($G = \bar{G}$) permits also the description of the kinetics as a whole. In fact, for a given ratio (here $x = 1$), h function will be studied. The similarity of the distribution as a function of time infers the f function knowledge for all particle diameters.

Specimens were sintered at 1100, 1150, and 1200 °C for dwell times varying between 30 min and 24 h for free-zirconia or doped tin dioxide-based ceramics. The growth kinetics were established from the grain size distribution (at least 300 grains) as a function of time, temperature. The corresponding experimental data have been reported in Fig. 2.

3.1.2. Grain growth mechanism

The growth rate calculation implies the determination of a mathematical representation for the curves of Fig. 2. In this way, the following equation was kept since it fit the most of kinetic curves:

$$G = G_0(1 + At)^{1/m} \quad (6)$$

where G_0 is the initial average grain size (at $t = 0$), G the average grain size (at t time), A and m correlation parameters that corresponds to the best correlation.

The used grain growth laws [23,27] have been established considering that the grain boundary movement should be slowed down when closed pores remain at the grain boundaries. Consequently, the grain growth kinetic is often regarded [23] as proportional to the average rate of the grain boundary

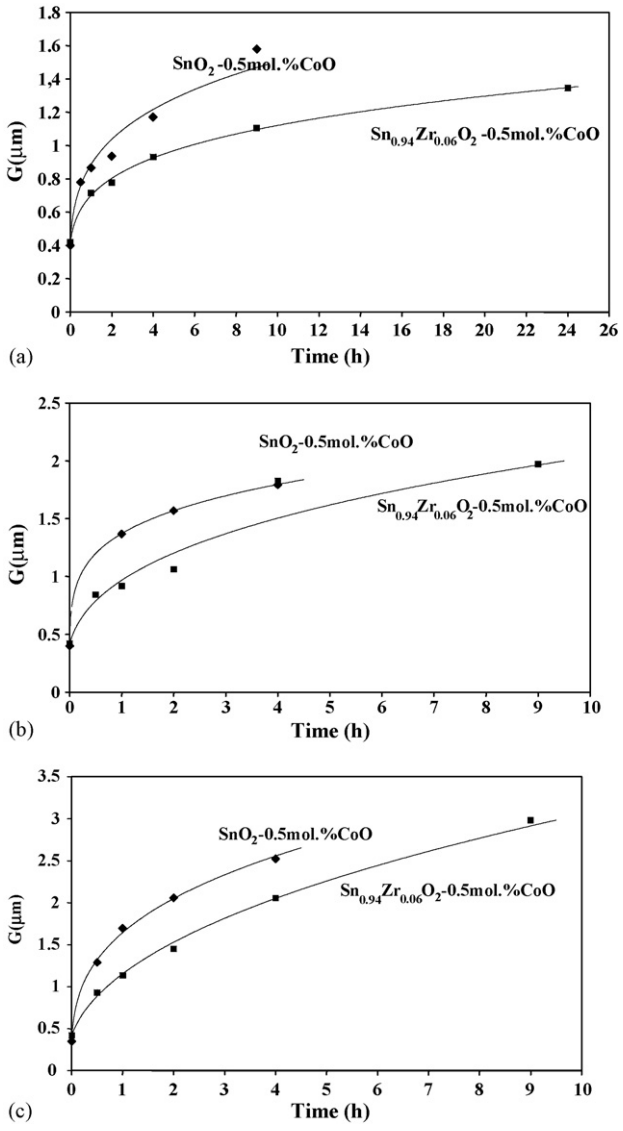

Fig. 2. $Sn_{0.94}Zr_{0.06}O_2$–0.5 mol% CoO and SnO_2–0.5 mol% CoO grain growth at different temperatures (1100, 1150, 1200 °C).

migration. Consequently, the rate of the grain boundary (V_g) could be expressed from the following equation [24–27]:

$$V_g = M_J(F_J - NF_P) = M_P F_P \quad (7)$$

where M_J, F_J are mobility and driving force of the grain boundary, respectively; N the pore density at the grain boundary and F_P the slowing down force due to the closed pores.Two cases must be considered:

- when the pore mobility controls the grain growth kinetic ($M_P \ll NM_J$)

$$V_g = \frac{dG}{dt} = \frac{k_G}{(1-\rho)^{m/3} G^{m-1}} \quad (8)$$

where ρ is the densification ratio at t time, k_G a kinetic constant, m an integer characterising the growth mechanism and G the average grain size at t time.

- when the grain boundary mobility limits the growth ($M_P \gg NM_J$)

$$V_g = \frac{dG}{dt} = \frac{k_G}{G^{m-1}} \quad (9)$$

The m values were varied between 2 and 4. The (dG/dt) and (dG/dt) $\times (1-p)^{m/3}$ expressions were plotted as a function of $1/G^{m-1}$. For each temperature and zirconium content (0 or 6%), the higher correlation coefficients (R) obtained for the regression straight lines relative to Eqs. (8) and (9) are reported in Table 4. Examples of dG/dt and (dG/dt) $\times (1-p)^{m/3}$ versus $1/G^{m-1}$ representation are given in Fig. 3.

For ZrO_2 free-SnO_2 materials and between 1150 and 1200 °C, the regression straight lines are best adjusted with values of $m = 4$ (surface diffusion) in the case of grain growth controlled by the pore mobility. At 1100 °C, no limiting step can be proposed for understanding the grain growth mechanism because the correlation coefficients are too weak.

With zirconia additives, the grain growth seems to be controlled by the grain boundary mobility: at the lower temperatures (1100 and 1150 °C), the limiting step consists in the second phase coalescence by diffusion process through the grain boundary ($m = 2$) whereas at the higher temperature (1200 °C) the grain boundary mobility may be blocked by precipitates ($m = 4$).

A kinetic law can be proposed for $Sn_{0.94}Zr_{0.06}O_2$–0.5 mol% CoO ceramic at 1200 °C

$$V_g = \frac{dG}{dt} = \frac{k_G}{G} \quad (10)$$

The grain growth values have been reported as a function of $1/G$ as shown in Fig. 4. The straight line so obtained intercepts the abscissa axis for the inverse of the critical grain size (G_C). This critical diameter (≈7 μm) corresponds to the grain size for

Table 4
Evolution of correlation coefficients for the Eqs. (8) or (9) and for the $Sn_{1-x}Zr_xO_2$–0.5 mol% CoO material (with $x = 0$ or 0.06)

Zirconia content in the solid-solution (%)	Temperature (°C)	Control by the grain boundary mobility			Control by the pore mobility		
		m	k_G (μm^m/h)	R	M	k_G (μm^m/h)	R
0	1100	4	0.150 ± 0.020	0.9460	4	0.040 ± 0.010	0.9090
	1150	2	0.221 ± 0.059	0.9343	4	0.007 ± 0.001	0.9995
	1200	2	1.660 ± 0.050	0.9991	4	0.049 ± 0.001	0.9994
6	1100	4	0.050 ± 0.005	0.9851	4	0.015 ± 0.003	0.9545
	1150	4	0.211 ± 0.027	0.9757	4	0.070 ± 0.016	0.8469
	1200	2	0.652 ± 0.040	0.9944	4	0.040 ± 0.005	0.9712

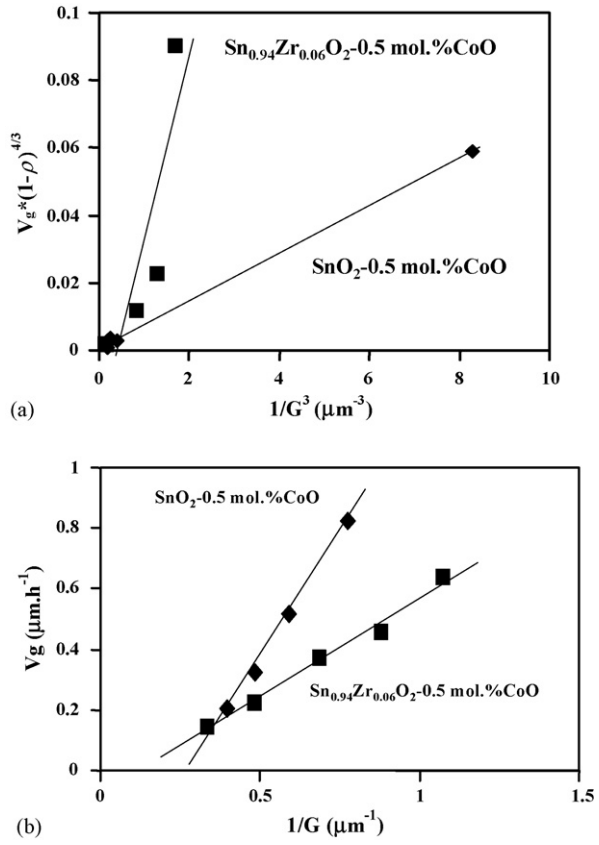

Fig. 3. $V_g^*(1-\rho)^{4/3}$ and V_g as a function of $1/G^3$ and $1/G$, respectively.

which the grain growth is ended. So, the growth kinetic at 1200 °C can be expressed by

$$\frac{d\bar{G}}{dt} = k\left(\frac{1}{\bar{G}} - \frac{1}{G_C}\right) \tag{11}$$

The integration of Eq. (10) provides the following expression:

$$\ln\left(\frac{G_C - G_0}{G_C - \bar{G}}\right) + \frac{G_0 - \bar{G}}{G_C} = \frac{k}{G_C^2}t \tag{12}$$

where G_0 represents the starting grain size, G_C the critical grain size and $\bar{G}$ the average grain size.

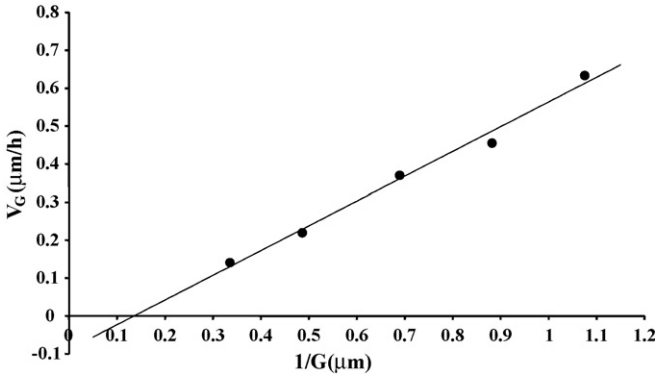

Fig. 4. Grain growth kinetics ($m = 4$) as a function of grain size.

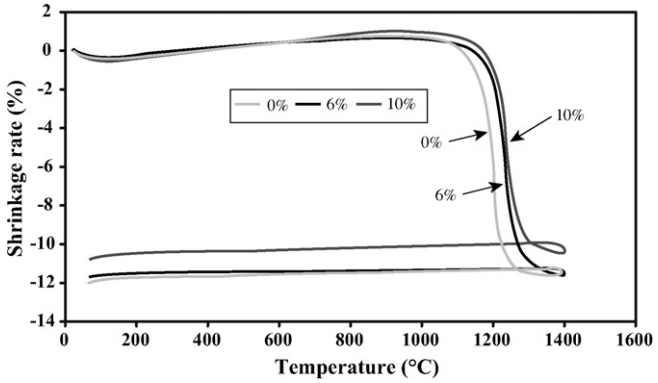

Fig. 5. Dilatometry results for $Sn_{1-x}Zr_xO_2$–0.5 mol% CoO ceramics ($\Delta L/L$) as a function of temperature and of zirconium content.

3.2. Densification

3.2.1. Densification kinetics

Fig. 5 shows dimension changes ($\Delta L/L$) versus temperature for dilatometry experiments carried out using a heating rate of 5 °C/min from room temperature to 1400 °C, then a cooling rate of 10 °C/min. From dilatometric curves, it appears that sintering densification of SnO_2–0.5 mol% CoO ceramic takes place between 1100 and 1400 °C. These results so obtained also confirm that zirconia additions retard the shrinkage appearance.

The densification kinetics of $Sn_{0.94}Zr_{0.06}O_2$–0.5 mol% CoO and SnO_2 ceramics have been obtained from dilatometric experiments in isothermal conditions. The shrinkage kinetics are given as a function of a corrected time that has been obtained by subtracting the heating time to the final time.

Fig. 6a–c gives the true densification kinetics of $Sn_{1-x}Zr_xO_2$ ceramics with $x = 0$ and 6 mol% for an isothermal treatment at 1100, 1150 and 1200 °C when the shrinkage rate is the highest. These curves clearly demonstrate that zirconia additions to SnO_2–0.5 mol% CoO inhibit the final densification rate. So, the maximum densification rate regardless the treatment temperature can reach 98% as opposed to 94% for SnO_2–0.5 mol% CoO and $Sn_{0.94}Zr_{0.06}O_2$–0.5 mol% CoO, respectively.

3.2.2. Densification mechanism

3.2.2.1. Densification as a function of time. In the case of sintering without liquid phase forming, the densification rate usually obeys to the following equation [28]:

$$\frac{d\rho}{dt} = \frac{AD}{(1-\rho)^{\alpha}RTG^n} \tag{13}$$

When the volume diffusion ($n = 3$ and $\alpha = 0$) plays the role of the rate limiting step, Eq. (13) becomes

$$\frac{d\rho}{dt} = 335\frac{D_v\gamma\Omega}{RTG^3} \tag{14}$$

or, when the rate-limiting step is the grain boundary diffusion ($n = 4$ and $\alpha = 1/2$)

$$\frac{d\rho}{dt} = 860\frac{D_j\delta_i\gamma\Omega}{(1-\rho)^{1/2}RTG^4} \tag{15}$$

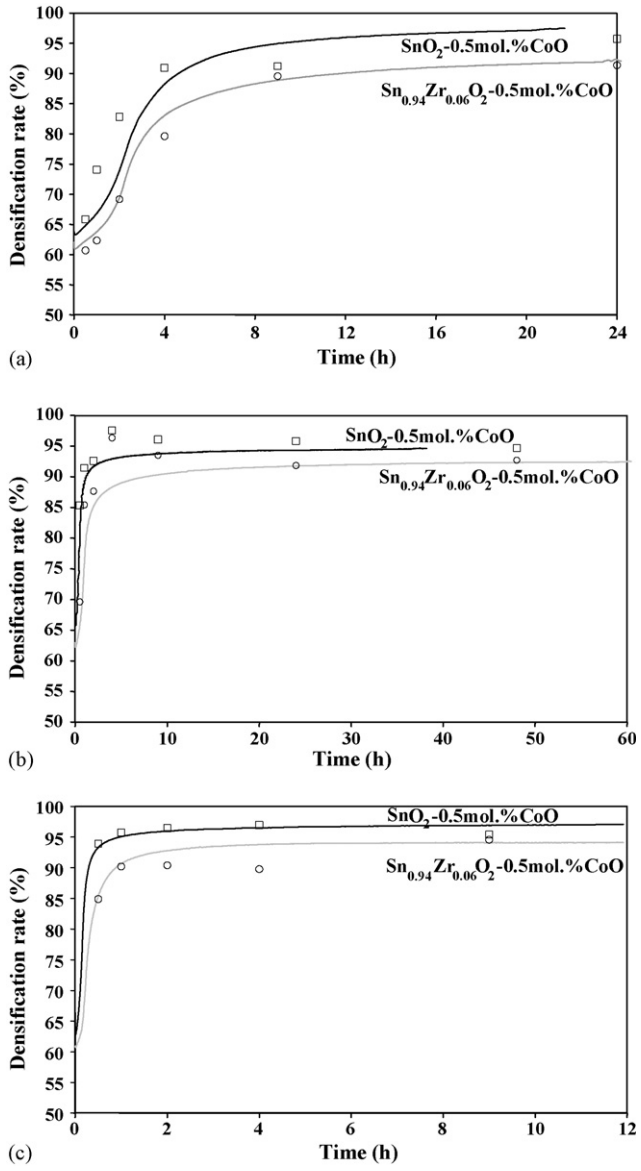

Fig. 6. Relative density as a function of time for SnO_2–0.5 mol% CoO and $Sn_{0.96}Zr_{0.04}O_2$–0.5 mol% CoO ceramics at 1100 °C (a), at 1150 °C (b) and at 1200 °C (c).

where $d\rho/dt$ is the densification rate, γ the solid–gas surface tension, D_v the volume diffusion coefficient, D_j the grain boundary diffusion coefficient, G the grain size, δ_i the grain boundary thickness, T temperature, Ω the molar volume, R a gas constant.

Eqs. (14) and (15) can be expressed as a function of time by taking into account the grain growth kinetics from Eqs. (8) and (9). Then as a function of n/m value, the integration of Eqs. (14) and (15) can lead to the following relative density expressions:

If $n > m$, for grain growth controlled by grain boundary mobility (t) or pore mobility (t^*)

$$\rho = 1 - \left[\frac{(1-\rho_0)^{\alpha+1} - (1-\rho_f)^{\alpha+1}}{(1 + t(\text{or } t^*)/t_i)^{(n/m-1)}} + (1-\rho_f)^{\alpha+1} \right]^{1/\alpha+1} \quad (16)$$

If $n = m$, for grain growth governed by grain boundary (t) or pore mobility (t^*)

$$\rho = 1 - \left[-(1-\rho_0)^{\alpha+1} - (1-\rho_f)^{\alpha+1} \times \ln\left(1 + \frac{t(\text{or } t^*)}{t_i}\right) + (1-\rho_f)^{\alpha+1} \right]^{1/\alpha+1} \quad (17)$$

where ρ is the relative density at t time (or at t^* time), ρ_0 the relative density at initial time, ρ_f the final density, t_i, n/m and α the sintering parameters. t^* is calculated from the following equation:

$$t^* = \int_0^t (1-\rho)^{-m/3}\, dt \quad (18)$$

where m represents the grain growth kinetic exponent that is reported in Table 4 for each temperature and zirconium content. Only the adequate theoretical expressions that permit fitting experimental data have been reported in Table 5.

From m and n/m ratio values (Table 5), it is possible to define more precisely the densification mechanism. For ZrO_2 free-SnO_2 at 1100 °C, when it is supposed that the grain boundary mobility controlled the grain growth (Eq. (9)), the densification exponent (n) tends to 7. Consequently, no densification mechanism can be associated to this value meaning that this hypothesis must be rejected. This result well confirms the previous observations of Section 3.1.2.

Conversely, when the pore mobility governs the grain growth kinetic (Eq. (8)), n value calculated from m exponent (equal to 4) is in a good agreement with one densification mechanism. So, it can be concluded that the grain growth depends upon the pore mobility and the corresponding limiting step consists in the surface diffusion whereas the densification is controlled by the grain boundary diffusion process. All of n and m values have been reported in Table 5. With regards to these data, it appears that the grain growth kinetic is controlled either by the pore mobility (for SnO_2–0.5 mol% CoO) or by the grain boundary mobility (for $Sn_{0.94}Zr_{0.06}O_2$–0.5 mol% CoO). The rate limiting step of the grain growth is the surface diffusion for ZrO_2 free-SnO_2 whereas the one of densification mechanism is either the grain boundary diffusion or the volume diffusion.

3.2.2.2. Densification kinetic as a function of grain size. The relative density of sintered samples studied in Section 3.1, i.e. for the determination of grain growth kinetic have been systematically determined. Globally, there is a good accordance between the densification kinetics obtained either from dilatometric tests or from the relative density measured by the Archimedes method.

The densification curves have been fitted by the following mathematical expression that corresponds to a sigmoid function:

$$\rho = \frac{\rho_i - \rho_f}{1 + (t/t_0)^p} + \rho_f \quad (19)$$

Table 5
Densification law parameters obtained from Eqs. (16) and (17) for $Sn_{0.94}Zr_{0.06}O_2$–0.5 mol% CoO and SnO_2–0.5 mol% CoO materials

	ρ_0	ρ_f	t_i (h)	n/m	α	R	Equation	n	R
SnO_2–0.5 mol% CoO									
1100 °C									
Grain boundary mobility	0.560	0.984	7.473	2.0	0	0.987	(20)	6.922	0.944
Pore mobility ($m = 4$)	0.587	0.973	11.560	0.9	0.5	0.999			
1150 °C									
Grain boundary mobility	0.608	0.943	1.017	2.306	0	0.984	(20)	4.327	0.946
Pore mobility ($m = 4$)	0.621	0.944	1.359	0.941	0.5	0.989			
1200 °C									
Grain boundary mobility	0.560	0.972	0.927	4.603	0	0.984	(20)	4.019	0.942
Pore mobility ($m = 4$)	0.576	0.974	0.522	1.003	0.5	0.991			
$Sn_{0.94}Zr_{0.06}O_2$–0.5mol% CoO									
1100 °C									
Grain boundary mobility	0.532	0.964	4.098	1.009	0.5	0.983	(20)	3.812	0.975
Pore mobility ($m = 4$)	0.571	0.917	32.597	1.426	0	0.994			
1150 °C									
Grain boundary mobility	0.541	0.931	0.650	0.979	0.5	0.992	(20)	3.752	0.986
Pore mobility ($m = 4$)	0.560	0.932	1.818	0.598	0	0.990			
1200 °C									
Grain boundary mobility	0.523	0.942	0.704	2.199	0.5	0.990	(20)	4.084	0.950
Pore mobility ($m = 4$)	0.510	0.961	0.262	0.449	0	0.978			

where ρ is the relative density at t time, ρ_0 the starting relative density, ρ_f the final relative density, t_0 a critical time, p a real exponent.

Otherwise, the calculation of n exponent that gives information on the densification mechanism results from the following equation (issued from Eq. (15)):

$$\ln\left(\frac{d\rho}{dt}\right) = a - n \times \ln(G) \tag{20}$$

The n values so obtained have been reported in Table 6. At 1100 and 1150 °C for ZrO_2 free-SnO_2 and $Sn_{0.94}Zr_{0.06}O_2$ ceramics, respectively, the n value (≈3) is not coherent with that determined from the densification kinetic law (Section 3.2.2.1). Conversely, at the others temperatures for both ZrO_2 free-SnO_2 and $Sn_{0.94}Zr_{0.06}O_2$ ceramics, the $n = 4$ value can be associated to a mass transfer by grain boundary diffusion for the densification mechanism. This result is a good agreement with the previous approach. Moreover, the representation that gives the densification rate evolution as a function of $1/G^n$ allows the determination of (k_d) kinetic constant from the slope (see Table 6).

3.3. Discussion

All of the results concerning the grain growth and densification mechanisms studies seem to be coherent:

(a) For ZrO_2 free-SnO_2 ceramic, regardless temperature, the grain growth law is controlled by the surface diffusion in pores. The growth law is obtained by integrating Eq. (8)

$$G = G_0\left(1 + \frac{4k_G}{G_0^4}\int_0^t (1-\rho)^{-4/3}\,dt\right)^{1/4} \tag{21}$$

At 1100 °C, the study of densification law versus time lead us to consider the grain boundary diffusion as the rate determining step of the densification mechanism. Nevertheless, the determination of densification kinetics as a function of grain size does not permit confirming this hypothesis. At 1150 and 1200 °C, the densification studies performed as a function of grain size and time indicate that the limiting step of densification mechanism is the grain boundary diffusion.

Table 6
Densification parameters obtained from densification kinetics for $Sn_{0.94}Zr_{0.06}O_2$–0.5 mol% CoO and SnO_2–0.5 mol% CoO materials between 1100 and 1200 °C

Zirconia content in the solid solution (%)	Temperature (°C)	n	k_d ($\mu m^n/h$)	R
0%	1100	2.799	0.0516	0.973
	1150	3.530	0.0072	0.958
	1200	4.451	0.0509	0.978
6%	1100	3.644	0.0012	0.946
	1150	1.707	0.0207	0.930
	1200	4.475	0.0369	0.993

(b) For $Sn_{0.94}Zr_{0.06}O_2$ ceramic, the grain growth obeys to the grain boundary mobility. After integration of Eq. (9), the corresponding growth kinetic can be written following:

$$G = G_0\left(1 + \frac{4k_G}{G_0^4}t\right)^{1/4}, \quad \text{at 1100 and 1150 °C} \tag{22}$$

$$G = G_0\left(1 + \frac{2k_G}{G_0^2}t\right)^{1/2}, \quad \text{at 1200 °C} \tag{23}$$

Independently of the sintering temperature, the densification studies as a function of time and grain size clearly revealed that the rate determining step was the grain boundary diffusion.

From theoretical laws, the sintering map ($G = f(\rho)$) enables to give an overall description of the SnO_2-based material sintering mechanism. For example, at 1150 and 1200 °C, the corresponding trajectory of theoretical sintering can be established from the ratio between the densification and grain growth kinetics:

(a) for ZrO_2 free-SnO_2 ceramic

$$\frac{d\rho/dt}{dG/dt} = \frac{k_d/(1-\rho)^{1/2}G^4}{k_G/(1-\rho)^{4/3}G^3} = \frac{k_d}{k_G}\frac{(1-\rho)^{5/6}}{G} \tag{24}$$

(b) for $Sn_{0.94}Zr_{0.06}O_2$ ceramic

$$\frac{d\rho/dt}{dG/dt} = \frac{k_d/(1-\rho)^{1/2}G^4}{k_G/G^3} = \frac{k_d}{k_G}\frac{(1-\rho)^{-1/2}}{G} \tag{25}$$

After integration, Eqs. (24) and (25) become

$$\rho = 1 - \left[-\frac{1}{6}\frac{k_d}{k_G}\ln\left(\frac{G}{G_0}\right) + (1-\rho_0)^{1/6}\right]^6 \tag{26}$$

$$\rho = 1 - \left[-\frac{3}{2}\frac{k_d}{k_G}\ln\left(\frac{G}{G_0}\right) + (1-\rho_0)^{3/2}\right]^{2/3} \tag{27}$$

For ZrO_2 free SnO_2 ceramics, the experimental data (grain size, relative density) are well restored by the previous model (Eq. (26)) at 1150 and 1200 °C as shown in Fig. 7. It can be noticed that Eq. (26) does not permit correctly fitting the experimental data for $Sn_{0.94}Zr_{0.06}O_2$ ceramic at 1150 and 1200 °C.

Previous studies deal with the role of additives [14,18,29–32] on the sintering process in solid state for SnO_2-based ceramics. When the content of sintering aids as CuO [14,29], MnO_2 [30] or ZnO [31] exceeds their solubility in the tin dioxide lattice, a segregation layer can appear around the tin dioxide grains. This second solid phase can strongly modify the matter transport at the grain boundary and, consequently, the grain growth and densification kinetics. These observations seem to be partly in accordance with those obtained for the SnO_2–0.5 mol% CoO ceramic between 1150 and 1200 °C. Indeed, the results of the present modelling indicate that the role of CoO as sintering agent mainly involves the grain boundary mechanism. So, the densification kinetic seems to

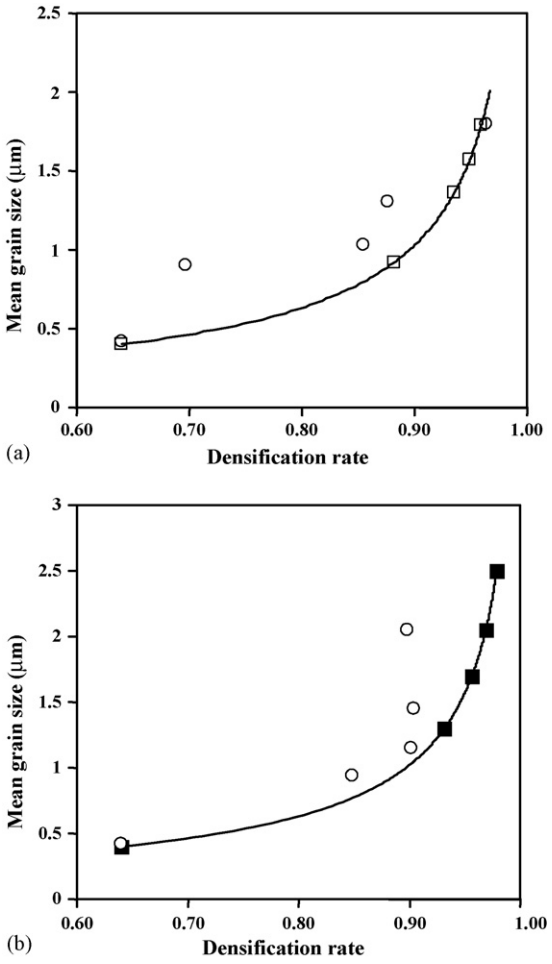

Fig. 7. Grain growth vs. densification rate for SnO_2–0.5 mol% CoO (■) and $Sn_{0.94}Zr_{0.06}O_2$–0.5 mol% CoO (○) at 1150 °C (a) and at 1200 °C (b).

be governed by the specie diffusion at the grain boundary. In this case, the intergranular phase is probably the spinell Co_2SnO_4 compound, which has been detected during previous investigations [13,32].

The effect of zirconia on the monoxide cobalt solubility in SnO_2–0.5 mol% CoO ceramics appears to be difficult to evaluate because the SnO_2–ZrO_2–CoO phase diagram is not well known. Consequently, at present, the evolution of the sintering mechanisms in presence of zirconia cannot be interpreted from the modification of the secondary phase properties.

4. Conclusion

The present study led to precise the rate determining step for grain growth and densification mechanisms in ZrO_2 free-SnO_2 and $Sn_{0.94}Zr_{0.06}O_2$ ceramics in isothermal conditions between 1100 and 1200 °C. So, for SnO_2–0.5 mol% CoO ceramic, the grain growth is controlled by the pore mobility and more particularly by the surface diffusion of species. For the same material, the rate limiting step of the densification is the grain boundary diffusion between 1150 and 1200 °C. This sintering modelling allowed restoring all of the experimental data (grain

size, densification rate) as it has been well shown by the corresponding sintering card.

In presence of zirconia, a discrepancy between experimental data and the present modelling has been detected. This could be explained, in a first time, by a modification of the secondary phase composition, i.e. of mass transfer kinetic and, in the second one, by the experimental uncertainties concerning the density measurements.

Acknowledgement

The authors are pleased to thank Lionel Aranda for technical help, especially during the dilatometry experiments.

References

[1] J.G. Fagan, V.R. Amarakoon, Am. Ceram. Soc. Bull. 72 (1993) 119.
[2] P.P. Tsai, I.C. Chen, M.H. Tzeng, Sens. Actuators B 14 (1–3) (1993) 610–612.
[3] N. Jaffrezic-Renault, C. Pijolat, A. Pauly, J. Brunet, C. Varenne, M. Bouvet, P. Fabry, Actualité Chim. 3 (2002) 157–171.
[4] R. Lalauze, C. Pijolat, G. Tournier, B. Breuil, Electr. Technol. 33 (1–2) (2000) 31–39.
[5] T.J. Coutts, X. Li, T.A. Cessert, IEEE Electron. Lett. 26 (1990) 660.
[6] T.J. Coutts, N.M. Persall, T. Tarricone, J. Vacuum Technol. Sci. B 2 (1984) 140.
[7] P.P. Deimel, B.B. Heimofer, E. Voges, IEEE Photon. Technol. Lett. 2 (1990) 499.
[8] N. Jakon, J. Ford, Thin Solid Films 77 (1981) 23.
[9] V.G. Panteleev, K.S. Ramm, T.I. Pron'kina, Glass Ceramics 46 (1990) 199.
[10] P. Olivi, E.C.P. Souza, E. Longo, J.A. Varela, L.O.S. Bulhoes, J. Electrochem. Soc. 140 (1993) 81–82.
[11] H.D. Joss, M.Sc. Thesis, University of Washington, Seattle, WA, 1975.
[12] E.R. Leite, J.A. Cerri, E. Longo, J.A. Varela, C.A. Paskocima, J. Europ. Ceram. Soc. 21 (2001) 669–675.
[13] A. Maître, D. Beyssen, R. Podor, J. Europ. Ceram. Soc. 24 (2004) 3111–3118.
[14] J. Lalande, R. Ollitrault-Fichet, P. Boch, J. Europ. Ceram. Soc. 20 (2000) 2415–2420.
[15] B. Gaillard-Allemand, R. Podor, M. Vilasi, Ch. Rapin, A. Maître, P. Steinmetz, J. Europ. Ceram. Soc. 22 (2002) 2303–2797.
[16] J.A. Varela, E. Longo, N. Barelli, A.S. Tanaka, W.A. Mariano, Ceramica 31 (1985) 241.
[17] J.A. Cerri, E.R. Leite, D. Gouvêa, E. Longo, J. Am. Ceram. Soc. 79 (3) (1996) 799–804.
[18] W.W. Mullins, J. Vinals, Acta Met. 41 (5) (1989) 1359–1367.
[19] B.D. Gaulin, S. Spooner, Y. Morii, Phys. Rev. Lett. 59 (6) (1987) 668–671.
[20] D.J. Srolovitz, M.P. Anderson, G.S. Grest, P.S. Sahni, Acta Met. 32 (9) (1984) 1429–1438.
[21] F.M.A. Carpay, S.K. Kurtz, Mater. Sci. Res. 11 (1978) 217.
[22] J. Ricote, L. Pardo, Acta Met. 44 (3) (1996) 1155.
[23] R.J. Brook, J. Am. Ceram. Soc. 52 (1969) 56–57.
[24] R.J. Brook, J. Am. Ceram. Soc. 52 (1969) 339–340.
[25] N.J. Shaw, Powder Met. Int. 21 (3) (1989) 16–21.
[26] F.A. Nicols, J. Appl. Phys. 37 (13) (1966) 4502–4599.
[27] F.A. Nicols, J. Am. Ceram. Soc. 51 (1968) 468–469.
[28] N.J. Shaw, Powder Met. Int. 21 (3) (1989) 16–21.
[29] D. Gouvea, A. Smith, J.P. Bonnet, J.A. Varela, J. Europ. Ceram. Soc. 18 (1998) 345–351.
[30] N. Dolet, J.M. Heintz, L. Rabardel, M. Onillon, J.P. Bonnet, J. Mater. Sci. 30 (1995) 365–368.
[31] T. Kimura, S. Inada, T. Yamaguchi, J. Mater. Sci. 24 (1989) 220–226.
[32] J.A. Varela, J.A. Cerri, E.R. Leite, E. Longo, M. Shamsuzzoha, R.C. Bradt, Ceram. Inter. 25 (1999) 253–256.